New Journal of Physics
The open access journal at the forefront of physics

Deutsche Physikalische Gesellschaft DPG
IOP Institute of Physics

Published in partnership with: Deutsche Physikalische Gesellschaft and the Institute of Physics

OPEN ACCESS

RECEIVED
7 July 2016

REVISED
1 October 2016

ACCEPTED FOR PUBLICATION
13 October 2016

PUBLISHED
4 November 2016

PAPER

The electronic structure of Tb silicide nanowires on Si(001)

S Appelfeller, M Franz, H-F Jirschik, J Große and M Dähne

Institut für Festkörperphysik, Technische Universität Berlin, Hardenbergstraße 36, D-10623 Berlin, Germany

E-mail: stephan.appelfeller@physik.tu-berlin.de

Keywords: nanowires, rare earths, silicide, electronic structure, one-dimensional metallicity

Abstract

The electronic structure of Tb silicide nanowires on planar and vicinal Si(001) surfaces was investigated using scanning tunneling spectroscopy, core-level photoemission spectroscopy, and angle-resolved photoemission spectroscopy. The nanowires are metallic and their formation results in a band bending corresponding almost to flatband conditions on n-type substrates. The chemical core-level shifts of the Si-2p spectral components of the nanowires are independent of the substrate offcut indicating the growth of identical nanowire structures. Using vicinal surfaces a single-domain growth of nanowires is possible, enabling the differentiation of the electronic band structure parallel and perpendicular to the nanowires. In this way, five quasi one-dimensional bands crossing or reaching the Fermi level are found.

1. Introduction

One-dimensional metals are known to show various unique physical properties and phenomena, e.g. Tomonaga–Luttinger liquid behavior or the Peierls instability [1–3]. Unfortunately, ideal, i.e. isolated, one-dimensional structures cannot be realized since they are inherently unstable. However, by embedding them in a three- or two-dimensional environment so called quasi one-dimensional systems may be stable and can be studied. Such systems were first realized using anisotropic crystals of organic charge transfer salts [4], but in recent years the research focused on quasi one-dimensional structures growing by self-organization on surfaces, where the interaction of the system with the environment can be more easily tuned [5–9].

A possible model system are Tb silicide nanowires on Si(001) surfaces. Their growth was analyzed in detail in our recent study [10]. They are prepared by depositing Tb on clean surfaces followed by an annealing procedure. Thereby, single nanowires or bundles of nanowires with grooves between individual nanowires are formed. Generally, a higher metal coverage as well as a higher annealing temperature promote the growth of bundled nanowires at the expense of single nanowires. In addition, an exclusive growth of parallel nanowires is possible when using vicinal substrates with sufficiently large offcut. Depending on the exact preparation conditions further structures may form in addition to the nanowires, e.g. a well ordered wetting layer forms at lower Tb coverage.

Tb silicide nanowires belong to the group of silicide nanowires of the trivalent rare earth metals, which are assumed to have very similar properties, e.g. they are described by the same structural model based on the hexagonal rare earth disilicides [11–15]. On the Si(111) surface, these disilicides grow epitaxially as two-dimensional metallic thin films and show very high Schottky barrier heights on p-type Si [16–18]. If the latter also persists for the nanowires on Si(001), these one-dimensional structures may be especially interesting for applications as electrically well decoupled one-dimensional connections in Si-based integrated circuits. Promisingly, initial studies showed that a passivation of the silicide nanostructures by Si overlayers is possible [19, 20].

The metallicity of rare earth silicide nanowires is well established by scanning tunneling spectroscopy (STS) [21–23], angle-resolved photoemission spectroscopy (ARPES) [24, 25], and by transport measurements [22, 23]. Interestingly, all reported band structures indicate a quasi one-dimensional electronic structure, but they seem

to differ for various rare earth metals, e.g. an electron-like band around $\overline{\Gamma}$ crossing the Fermi level (E_F) was observed for Dy and Er, but not for Gd [24, 25].

This report represents an STS, core-level photoemission spectroscopy (XPS) and ARPES study on the electronic structure as well as the chemical properties of Tb silicide nanowires on Si(001) surfaces. Using STS, the expected metallicity of the nanowires could be confirmed. Least-squares fits of Si-2p spectra reveal components with practically the same core-level shifts and similar spectral weights for nanowires on planar and vicinal Si(001) substrates demonstrating that the nanowires are structurally identical. Furthermore, the band bending for the nanowire samples is characterized by nearly flat-band conditions on n-type Si, similar to the case of the Tb disilicide films on Si(111) [17]. The ARPES measurements on parallel nanowires using vicinal substrates reveal electronic bands crossing or reaching the Fermi level that disperse mainly parallel to the nanowires. The corresponding Fermi surfaces show slightly oscillating contours of the bands indicating a quasi one-dimensional electronic structure.

2. Experimental details

Planar and vicinal Si(001) substrates were cut from p-type and n-type Si wafers with offcut orientations of 0°, 4°, and 6° towards [110]. They were cleaned by flash annealing to about 1150 °C and, subsequently, slowly cooled down to get well ordered surfaces showing a 2×1 reconstruction and a low defect density, as controlled by scanning tunneling microscopy (STM). For this purpose, the substrates were resistively heated and their temperature was controlled using an infrared pyrometer (accuracy ±20 °C). Tb was deposited at room temperature using home-built electron beam evaporators and the coverage was determined by the deposition time and the deposition rate, which was calibrated using a quartz crystal microbalance (accuracy ±20%). Coverages are given in monolayers (ML), where 1 ML corresponds to 6.8×10^{14} atoms cm^{-2}. To enable the silicide formation, the samples were annealed at 450 °C–600 °C for 2 min. During the whole preparation process the pressures in the preparation chambers remained below 2×10^{-7} Pa. All measurements were performed *in-situ* in separate chambers with base pressures below 10^{-8} Pa.

STM and STS experiments were carried out using a home-built microscope operating at room temperature and a SPECS Nanonis control electronics. Electrochemically etched W tips were used, which were cleaned *in-situ* by electron bombardment. STM images were processed using the WSXM software [26]. Scanning tunneling spectra were taken as point spectra and the differential conductivity (dI/dV) was measured directly using lock-in techniques.

Another chamber system was used for the photoemission experiments at the UE56/2 PGM-1 beamline at BESSY II. The photoelectrons were analyzed using a SPECS PHOIBOS 100 electron analyzer equipped with a two-dimensional CCD detector. While most data were obtained at room temperature, the photoemission experiments were partially performed with liquid N_2 cooling for better resolution.

3. Results and discussion

3.1. Scanning tunneling microscopy and spectroscopy

Figure 1 gives an overview on the structures discussed during the course of this report. Independent of the used tunneling conditions, the nanowires generally appear as protrusions with huge aspect ratios and rather flat and structureless surfaces in STM already indicating metallicity. On planar samples (see figures 1(a)–(c)), a two domain growth of the Tb silicide nanostructures is observed due to the rotation of the surface structure by 90° with each monoatomic step. In contrast, a nearly single domain growth of the nanowires is found on vicinal Si(001) samples with sufficiently large offcut angles since the dominant formation of double steps leads to an identical orientation of the surface termination on most terraces (see figure 1(d)). Although structural differences of the nanowires on planar and vicinal substrates due to the presence of the double steps cannot be excluded by STM alone, the nanowires appear very similar and agree in most characteristics indicating the growth of identical nanowires, e.g. they show similar apparent heights and may form bundles of multiple nanowires [10]. The proposed structure model of the nanowires is shown in figure 1(e).

While this work mainly focuses on the Tb silicide nanowires, a Tb induced wetting layer may stay partially intact after the nanowire formation. Thus, XPS and ARPES data on the wetting layer were also taken to identify its influence on the data of the nanowire samples. The wetting layer, marked by the arrow in figure 1(a) and shown in figure 1(b), forms a 2×7 reconstruction on planar Si(001) surfaces and is characterized by linear features with significantly lower apparent heights than Tb silicide nanowires [10].

In order to obtain a large signal from the nanostructures in our photoemission studies, they have to cover a large part of the surface. When optimizing the preparation parameters, an almost complete coverage of the

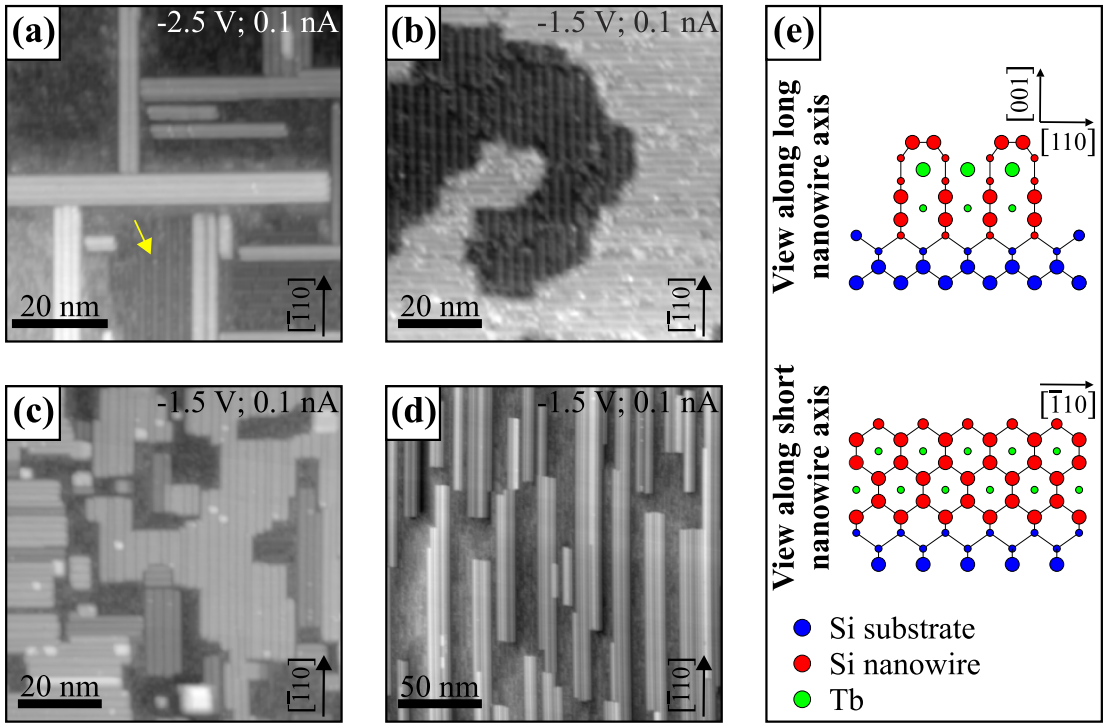

Figure 1. (a) Filled states STM image of a planar Si(001) surface showing single and bundled Tb silicide nanowires as well as wetting layer patches, e.g. in the area indicated by the yellow arrow (1.0 ML Tb annealed at 550 °C). (b) Filled states STM image of a planar Si(001) surface completely covered by the wetting layer (0.5 ML Tb annealed at 450 °C). (c) and (d) Filled states STM images of preparations with high nanowire surface densities on (c) a planar Si(001) surface and (d) a vicinal Si(001) surface with 6° offcut towards [110] (both: 1.5 ML Tb annealed at 600 °C). The tunneling conditions are given in the images. (e) Structure model of Tb silicide nanowires [10, 12, 27].

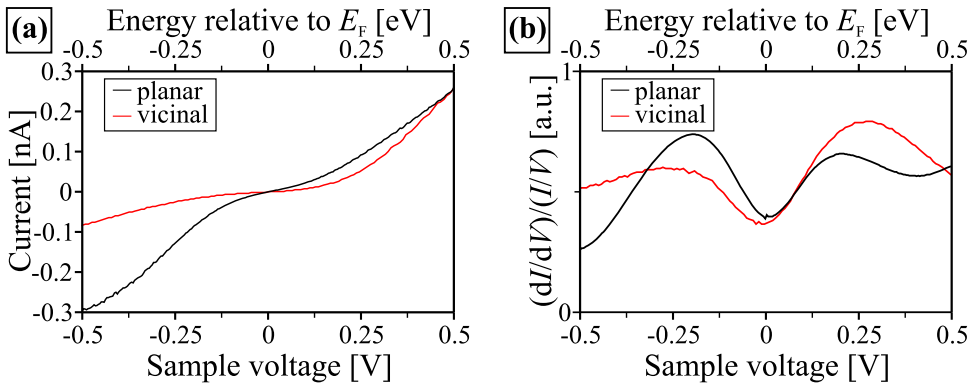

Figure 2. (a) Averaged I–V spectra and (b) averaged spectra of the normalized differential conductivity $((dI/dV)/(I/V))$ measured on a Tb silicide nanowire of a nanowire bundle on a planar Si(001) surface (black curve) and on a single nanowire on a vicinal Si(001) surface with 6° offcut towards [110] (red curve). It should be noted that different stabilizing conditions prior to the measurements were used (planar: 1 nA at 1.5 V and the tip approached towards the sample by 75 pm; vicinal: –0.1 nA at –1.5 V and the tip approached towards the sample by 100 pm), resulting in different slopes of the I–V spectra in (a), while the $(dI/dV)/(I/V)$ spectra in (b) are similar.

surface with the wetting layer as well as a surface coverage of up to 75% (50%) with Tb silicide nanowires on planar (vicinal) Si(001) surfaces is possible (see figures 1(b)–(d)) [10].

When positioning the metallic tip above a Tb silicide nanowire and measuring a current–voltage (I–V) spectrum, a metallic behavior is observed as shown in figure 2(a) for a nanowire within a bundle on a planar Si(001) surface as well as a single nanowire on a vicinal Si(001) surface. Both spectra show a nonzero slope at zero sample voltage indicating states at the Fermi level. This is further illustrated by the calculation of the normalized differential conductivity shown in figure 2(b), which represents a measure of the local density of states (LDOS) [28, 29]. In addition to the finite LDOS at the Fermi level (zero voltage), maxima are observed at about −0.25 eV and +0.25 eV. While such maxima are usually observed in single spectra, their exact energetic positions vary

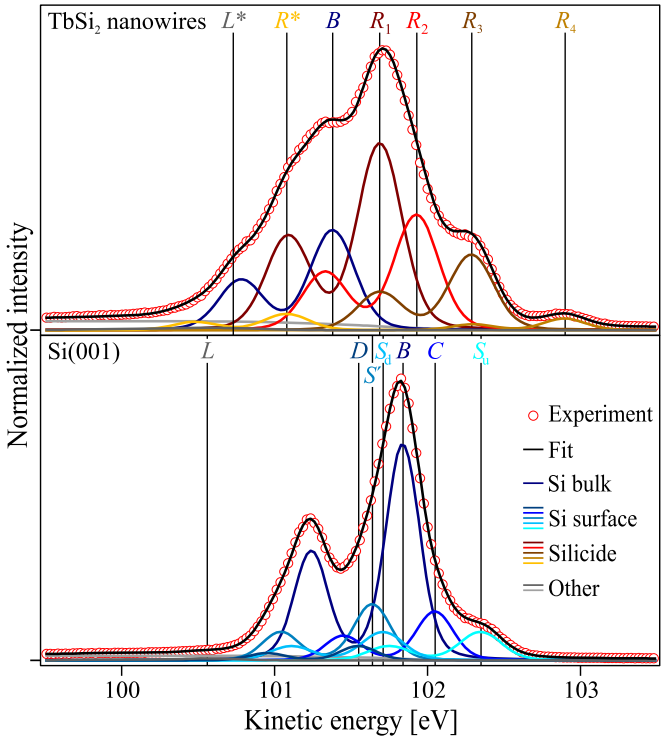

Figure 3. Si-2p spectra of a clean planar n-type Si(001) substrate (bottom) and of the same substrate with nanowires (top), both obtained at room temperature (photon energy $h\nu = 200$ eV). Strong changes in spectral shape as well as a shift of the bulk substrate component due to a change in band bending are observed. For the nanowire preparation, 1.7 ML Tb were deposited and annealed at 550 °C.

strongly with the tip location even for the same nanowire, so that the corresponding maxima of the averaged spectra appear broader. Similarly, nonuniform scanning tunneling spectra were found for YSi_2 nanowires [30]. Nevertheless, a metallic behavior was observed for all investigated Tb silicide nanowires independent of their growth as single or bundled nanowires, on both planar and vicinal Si(001) surfaces. Such a universal behavior may indicate the growth of identical nanowires in agreement with the STM results [10].

3.2. Core-level photoemission spectroscopy

A more unambiguous technique to control the equality of structures is XPS since identical structures are characterized by similar core-level shifts and relative intensities of the spectral components. Figure 3 shows room temperature Si-2p spectra of a planar Si(001) sample with and without nanowires. Thereby, the use of data obtained at room temperature enables us to estimate the band bending without having to consider photovoltage and charging effects, which may be present at low temperatures due to the reduced conductivity of the overlayers and of the Si substrates. Nevertheless, low temperature measurements were also performed to quantify the core-level shifts with higher precision. For most samples, XPS spectra with different surface sensitivities were acquired at photon energies of 200 eV, 160 eV, and 130 eV corresponding to kinetic energies of the photoelectrons of about 100 eV, 60 eV, and 30 eV, respectively, providing information for the correct assignment of the spectral components.

All Si-2p spectra shown in this work are normalized to equal heights. To analyze the spectra, they were least-squares fitted using spin-orbit split Voigt profiles to include both lifetime and instrumental broadening. To reduce the number of fit parameters, a fixed spin-orbit splitting of 0.60 eV and a fixed intensity ratio of 2:1 were used. For every spectrum a constant Lorentzian width of 0.07 eV–0.10 eV (full width at half maximum) was used for all peaks. The Gaussian widths of the peaks were between 0.30 eV and 0.40 eV, unless specified otherwise. A constant as well as a Shirley-type background were used, but no asymmetric line shapes had to be considered, consistent with previous findings [31–34]. For different photon energies, the spectra of the same sample were fitted until good results were obtained with differences of chemical shifts of the identical components below 0.03 eV.

The Si-2p spectrum of planar clean Si(001) is already well studied [31–33]. The bulk silicon component (B), components originating from the Si dimer surface reconstruction (S_u upper dimer atoms and S_d lower dimer atoms; restricted in the fit to identical intensities), as well as components of strained subsurface Si atoms (S' and C) are clearly identified. Additionally, there are two components (L and D) usually with rather low intensities,

Table 1. Overview on the derived absolute kinetic energies of the Si bulk component ($h\nu = 200$ eV) and the core-level shifts of the other components for the Si-2p XPS spectra of clean substrates shown in figure 4(a), with the respective peak labeling and literature values for comparison [33]. In addition, the average core-level shifts of all measurements including low temperature measurements (LTM) are given with their standard deviations. All values are given in eV.

	L	D	S'	S_d	B	C	S_u
Planar	−1.28	−0.29	−0.20	−0.13	101.84	0.21	0.51
4° offcut	−1.20	−0.29	−0.23	−0.13	101.78	0.20	0.51
6° offcut	−1.08	−0.34	−0.20	−0.15	101.83	0.21	0.49
Average (including LTM)	−1.20 ± 0.08	−0.33 ± 0.05	−0.22 ± 0.02	−0.14 ± 0.01		0.20 ± 0.02	0.49 ± 0.02
Eriksson and Uhrberg [33]	−1.34	−0.30	−0.22	−0.13		0.22	0.49

whose origins are still under debate (for more details regarding the component assignment see [33]). Fitting the spectrum of the clean planar substrate shown in figure 3, core-level shifts agreeing very well with the literature are observed (see table 1) [32, 33]. Additionally, the dependence of the peak intensities on the photon energy agrees very well with the component assignment (see figure 4(b)). For $h\nu = 200$ eV, the excited electrons have a larger mean free path than for $h\nu = 160$ eV [35]. Thus, the bulk component has a larger relative intensity for $h\nu = 200$ eV while surface components, e.g. the one of the dimers, have a larger relative intensity at $h\nu = 160$ eV. The difference between $h\nu = 160$ eV and $h\nu = 130$ eV is more difficult to interpret since the variation of the inelastic mean free path in the corresponding kinetic energy regime is not as clear [35]. Nevertheless, the increasing relative intensity of the dimer components with decreasing photon energy indicates increasing surface sensitivity. It should be noted that the Gaussian width of the L component is usually much larger than the ones of the other components [32, 33]. Furthermore, the Gaussian width of the B component of 0.28 eV is significantly smaller than the ones of the other components.

For vicinal samples, the general line shapes of the Si-2p spectra are very similar to the ones of planar samples (see figure 4(a)). Only a slight intensity reduction at high kinetic energies and a small intensity increase at low kinetic energies are observed. Indeed, the analysis of the spectra shows core-level shifts in very good agreement with the ones of the planar sample (see table 1). Thus, although new Si sites at the double steps are introduced, their concentration is too low and/or their core-level shifts are too close to already accounted ones to observe new spectral components. Furthermore, the relative intensities of the observed components show similar dependences on the photon energy (see figure 4(b)) and the kinetic energies of the bulk photoelectrons are comparable indicating very similar surface band bending. Merely, the core-level shift of the L component reduces towards the bulk component with increasing offcut angle and therewith also makes the position of the D component more uncertain. Due to the unknown origin of the L component, we refrain from speculating about the reason for this movement. Averaging these observed core-level shifts and also including further measurements, e.g. low temperature measurements, leads to very low standard deviations for all but the L and D components confirming the analogy of planar and vicinal samples.

The planar sample with silicide nanowires shows a broadening of the Si-2p spectrum and a shift of the spectral weight towards lower kinetic energies already indicating a shift of the Fermi level position (see figure 3). Even though we are mainly interested in the spectrum of the nanowires, all samples contain a mixture of the uncovered Si surface, the wetting layer, and nanowire structures, as illustrated schematically in figure 5. To reduce the influence of the other surface structures, preparation conditions with a high surface coverage by nanowires were chosen (compare preparation conditions in figures 1(c) and 3). Furthermore, every structure contains various different Si atom positions with different bonding configurations. For the nanowires, there are silicide surface Si atoms, silicide bulk Si atoms, silicide side Si atoms etc (see also the structure model in figure 1(e)). Due to this manifold of different Si sites, we do not expect to be able to fully assign all spectral components, but we may still identify major contributions, study the influence of the substrate vicinality, and, in particular, we may be able to derive the band bending behavior.

The nanowire Si-2p spectra on the different substrates show clear differences (see figure 6(a)). Nevertheless, all these spectra consist of six main components that have very similar core-level shifts for the different samples (see table 2). The differences of the spectra then solely result from different intensities of these components. Using fewer components may be possible for single spectra, but never allows a satisfactory fit of all spectra of one sample taken at different photon energies. In contrast to the spectra of the clean surfaces, where the substrate bulk component had a smaller Gaussian width than the other components, the nanowire spectra do not generally contain such a narrow component indicating that the substrate bulk component is broadened. In addition to the six main components, a component with rather low kinetic energy was found (L^*) for most nanowire spectra. Similar to the L component of the clean surfaces, this component always has a very low or even vanishing intensity and a large Gaussian width and will not be further discussed due to its unknown origin.

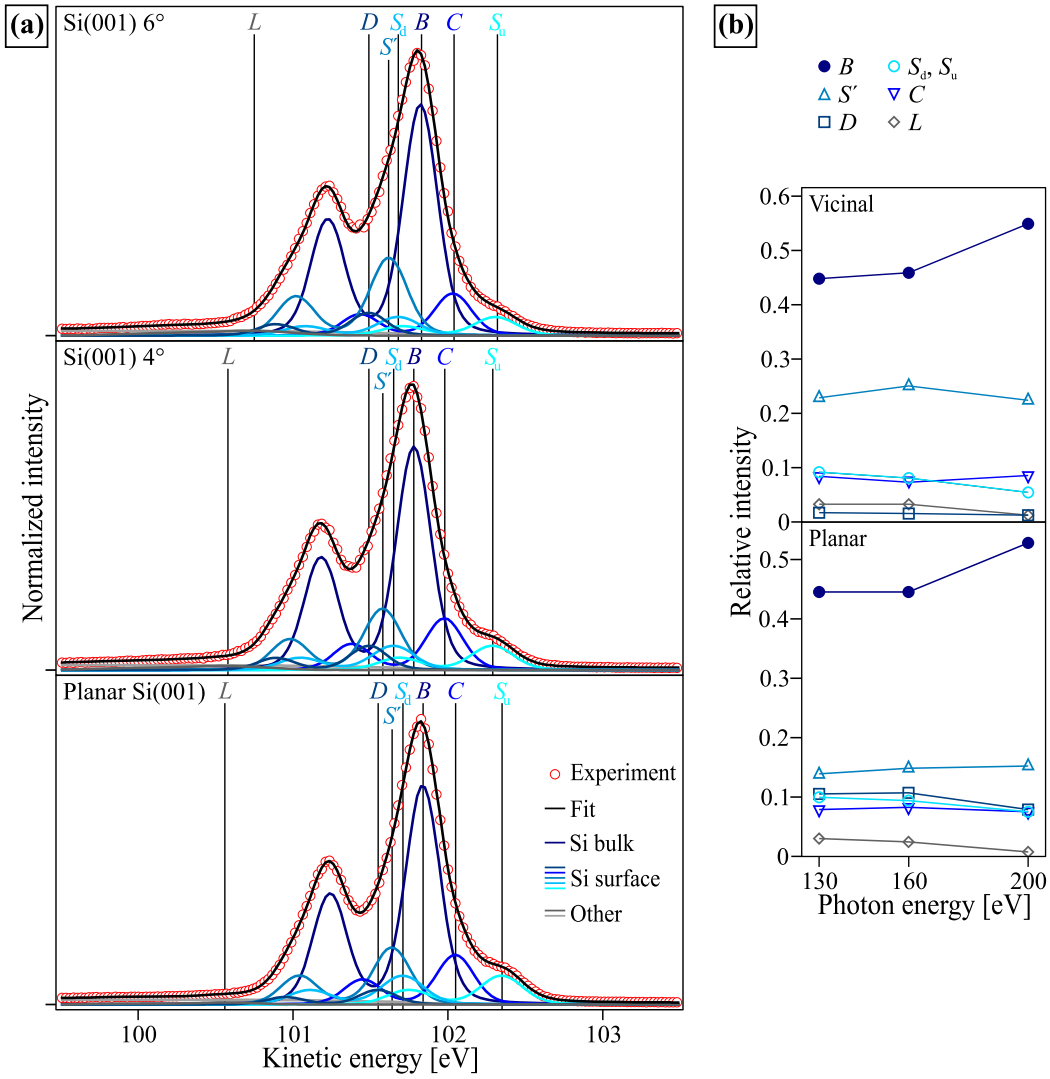

Figure 4. (a) Si-2p spectra of clean n-type Si(001) substrates with different offcut angles towards [110] obtained at room temperature ($h\nu = 200$ eV). (b) Exemplary intensity dependences of the Si-2p spectral components on the photon energy for clean Si(001) surfaces with 0° and 4° offcut towards [110]. The error of the relative intensities is lower than the heights of the symbols for all cases (including the intensity diagrams in the following figures).

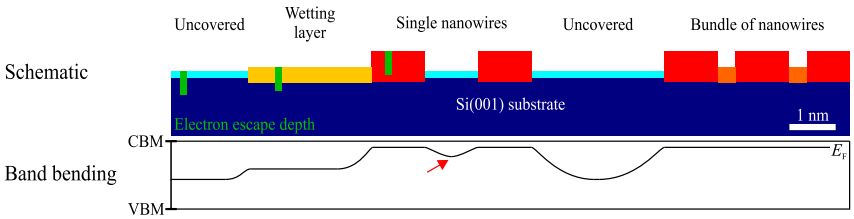

Figure 5. Schematic illustration of a Si(001) surface covered partly by Tb silicide structures. On nanowire samples, all structures form with various surface coverage ratios. Furthermore, the influence of the structures on the band bending is shown (CBM = conduction band minimum and VBM = valence band maximum). Thereby, the band bending of the clean substrate and of the wetting layer is screened in the vicinity of the nanowires by the high density of states of the metallic nanowires. Since such screening lengths on Si(001) are in the order of 1 nm [36, 37], this leads to large surface areas where the Fermi level position is significantly dominated by the one of the nanowires due to the dense nanowire growth (see figures 1(c) and (d)), which is illustrated above between the single nanowires (red arrow). Additionally, a photoelectron escape depth of 0.5 nm, being the typical inelastic mean free path for electrons with a kinetic energy of 100 eV in Si [35], is marked for the various surface structures.

Now, we discuss the observed spectral components in more detail. Thereby, it should be taken into account that the discussion of the weaker components is difficult since their intensity strongly depends on certain assumptions of the fit procedure, e.g. background shape, neighboring spectral components, or the symmetry of the line shape.

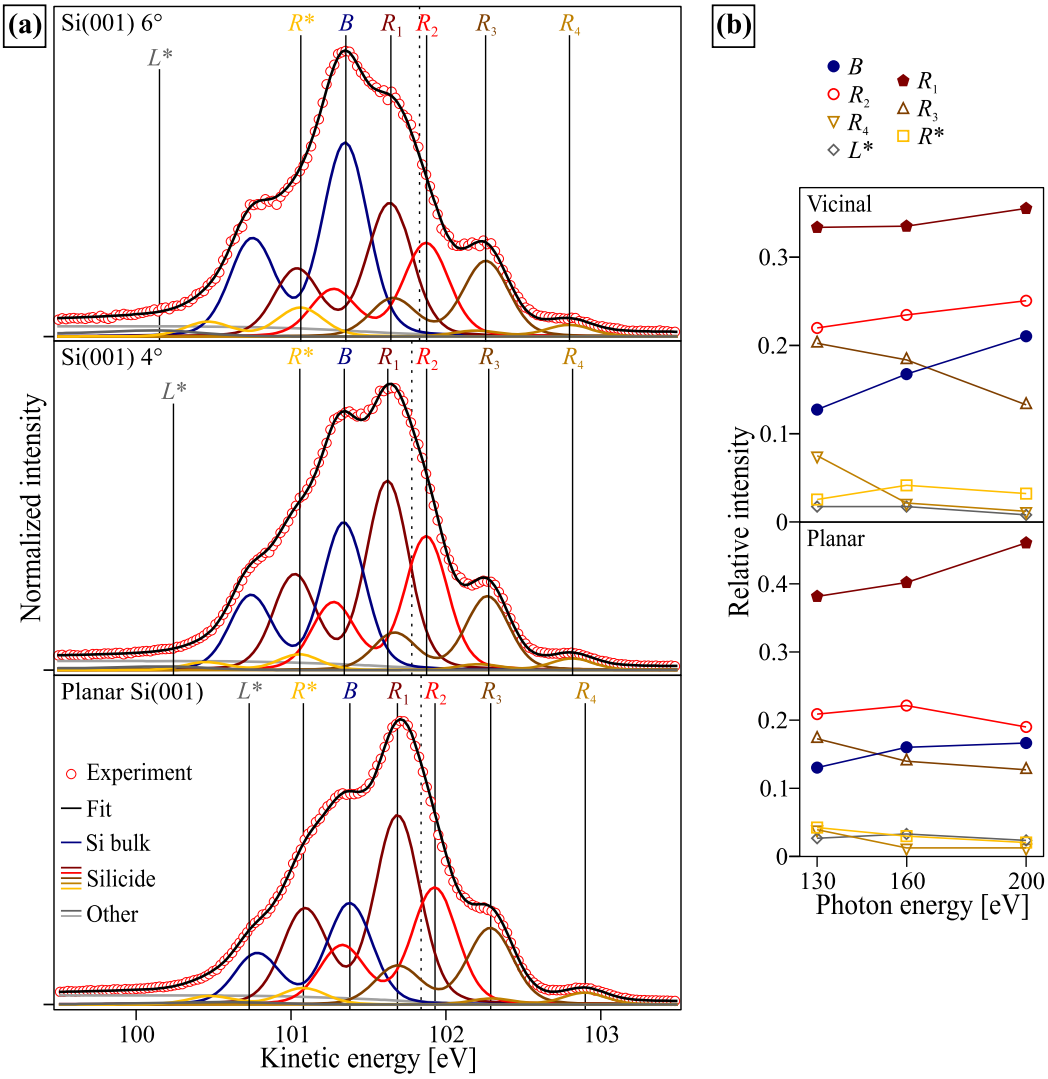

Figure 6. (a) Room temperature Si-2p spectra of the same substrates as in figure 4(a), but now covered with nanowires ($h\nu = 200$ eV). For the nanowire preparations, 1.7 ML and 1.5 ML Tb were deposited on the planar and vicinal samples, respectively, and annealed at 550 °C. The dashed lines indicate the bulk component positions found for the respective clean substrates. (b) Exemplary intensity dependences of the Si-2p spectral components on the photon energy for nanowire samples on substrates with 0° and 4° offcut towards [110]. These nanowire samples were prepared by deposition of 1.5 ML and 1.2 ML Tb on the planar and vicinal sample, respectively, and annealing at 550 °C.

Table 2. Overview on the derived absolute kinetic energies of the Si bulk component for the Si-2p spectra shown in figure 6(a) and the derived Si-2p core-level shifts of the spectral components of the nanowire and the wetting layer with respect to the Si bulk component (see XPS spectra in figures 6(a) and 7) with the respective peak labeling and literature values for Dy silicide nanowires for comparison [34]. All values are given in eV and '—' assigns non-observed components.

	L^*	R^*	B	R_1	R_2	R_3	R_4
Planar	−0.65	−0.30	101.38	0.29	0.55	0.89	1.52
4° offcut	−1.10	−0.29	101.35	0.28	0.53	0.93	1.47
6° offcut	−1.20	−0.29	101.36	0.29	0.52	0.9	1.44
Average (with LTM)	−1.0 ± 0.3	−0.30 ± 0.02		0.29 ± 0.01	0.54 ± 0.02	0.90 ± 0.03	1.46 ± 0.05
Vandré [34]	—	−0.28		0.30	0.61	1.10	1.50
Wetting layer (average)	−1.1 ± 0.1	−0.30 ± 0.02		0.30 ± 0.02	0.54 ± 0.02	1.17 ± 0.02	—

The B and R_1 components show a clear bulk-like behavior in all measurements with decreasing intensity for increasing surface sensitivity (decreasing photon energy) (see figure 6(b)). Thus, we may assume that they originate from the bulk substrate and the deeper regions of the nanowires. Due to the higher electronegativity of Si compared to the one of Tb [38], an electronic charge transfer from Tb to Si is expected in the nanowires. This

results in a shift to lower binding energies and therewith higher kinetic energies for the nanowire Si-2p levels with respect to the substrate Si-2p level as already found for RE silicides on Si(111) [16, 39]. Thus, the B component is assigned to the substrate and the R_1 component to the bulk of the nanowires.

In addition to these two bulk-like components, three components are observed at higher kinetic energies (R_2, R_3, and R_4). Of these components, only the one labeled R_4 shows an unambiguous dependence on the surface sensitivity for all measurements on planar and vicinal substrates. A strong intensity decrease towards larger escape depths is observed, so that we may assign R_4 to the surface dimers of the nanowires (see figures 1(e) and 6(b)). R_2 and R_3 cannot be assigned as easily due to non-monotone intensity variations with surface sensitivity for some of our measurements (see R_2 in figure 6(b)), but in general more bulk-like and more surface-like characteristics are found for R_2 and R_3, respectively. A possible reason for the non-monotone intensity variations is that the components consist of multiple unresolved subcomponents from the surface and from deeper regions.

The remaining component (R^*) lies at lower kinetic energies with respect to the substrate bulk component in contrast to the expectations for Si atoms in the vicinity of rare earth atoms. Since the component cannot be well assigned to the outermost Si atoms due to its non-monotone response to a changed surface sensitivity (see figure 6(b)), we may exclude oxidation or other contamination effects influencing mainly the outermost atoms. Similar to the S' component of the clean substrates, the R^* component may originate from strained subsurface Si atoms. Large strain effects due to Tb disilicide nanowire formation on Si(001) were recently observed in reflection anisotropy spectroscopy measurements [40]. Nevertheless, the wetting layer or uncovered surface areas, where the D component has a similar core-level shift with respect to the B component, cannot be excluded as possible origins of the R^* component.

Comparing the intensities (I) of the components unambiguously assigned to the nanowires (R_1, R_2, R_3, and R_4), rather similar ratios are derived for all nanowire samples, e.g. $I(R_1) : I(R_2) : I(R_3)$ is about 5 : 3 : 2 and $I(R_4) \ll I(R_3)$ for $h\nu = 200$ eV (see figure 6). No perfect agreement between all samples is expected due to the variation of the surface morphology with each sample. However, these similar intensity ratios and the small standard deviations of the core-level shifts clearly indicate the growth of identical nanowires on Si(001) substrates independent of their vicinality. Correspondingly, the large shape differences observed for the Si-2p spectra shown in figure 6(a) can be mainly attributed to an increase of the relative intensity of the substrate bulk component with increasing vicinality.

From the substrate bulk components of the nanowire Si-2p spectra, we can estimate the band bending at the Si substrate surface due to the presence of the nanowires using the shift of the kinetic energies of the substrate photoelectrons (see figures 3 and 6(a), tables 1 and 2). Assuming a Fermi level position of (0.48 $\pm$ 0.02) eV above the valence band maximum for clean n-type Si(001) being the average of previously reported Fermi level positions [34, 41, 42], the resulting shift of (0.45 $\pm$ 0.01 eV) leads to a Fermi level position of about 0.93 eV above the valence band maximum. Similar high Fermi level positions are characteristic for hexagonal rare earth disilicide monolayers on Si(111) [16–18]. Thus, the band bending behavior indicates the growth of an analogous silicide for the nanowires on Si(001) as for thin films on Si(111), in accordance with the assumed structure model (see figure 1(e)).

It should be noted here that this rather extreme Fermi level position deviates strongly from the usual position at the charge-neutrality level close to midgap, which may be ascribed to metal induced gap states [43–45]. However, in the present case the density of states of the nanowires in the Si band gap may be small, as also observed for the silicide monolayers on Si(111) [16–18], leading to a minor influence of metal induced gap states. Instead, the Fermi level position can rather be ascribed to the low work function of the rare earth silicide according to the model originally proposed by Schottky [46].

The slight deviation from the Fermi level position reported for Si(111) substrates may be related to the different growth modes. On Si(111), large patches of the monolayer silicide in between extended, well ordered clean surface areas are observed leading to a splitting of the observed substrate Si-2p level in a shifted and an unshifted component [17]. In contrast, the nanowire structures on Si(001) are higher (about 0.7 nm [10]) than the silicide monolayer on Si(111) (about 0.4 nm [47]) leading to a decreased intensity of the completely shifted substrate component. Furthermore, the surface areas in between nanowires are disordered and much narrower than in between the monolayer patches on Si(111) (see figures 1(c) and (d)), resulting in relative large contributions from surface areas close to the nanowires, where the band bending of the free surface is almost completely screened by the high density of states of the metallic nanowires (see red arrow in figure 5). In addition, such screening processes are also expected for the patches of the non-metallic wetting layer, which may be present on the nanowire samples and exhibit a Fermi level position in between that of the clean surface and that of the nanowires (see below and figure 5). Thus, the substrate component of the nanowire samples is expected to shift to higher kinetic energies than the one expected directly under the nanowires, and is also expected to have a larger Gaussian width than the one of the clean surfaces, consistent with our findings. This

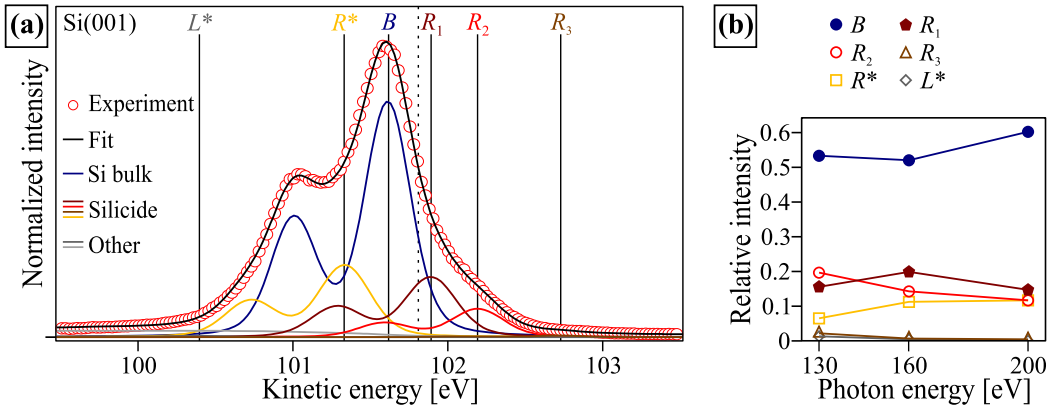

Figure 7. (a) Room temperature Si-2p spectrum for a wetting layer sample ($h\nu = 200$ eV; planar Si(001) with 0.5 ML Tb annealed at 500 °C). (b) Exemplary intensity dependences of the Si-2p spectral components of the wetting layer on the photon energy (planar Si(001) with 0.4 ML Tb annealed at 450 °C).

view is further supported by the lack of a dominant contribution at the kinetic energy of the substrate component of the clean surfaces (see figure 6(a)).

The observation of these six main components of the Si-2p nanowire spectra and their assignment nicely agrees with earlier XPS results reported for Dy induced nanostructures on Si(001) [34]. Interestingly, the observed core-level shifts are rather similar for Tb and Dy, again illustrating the chemical similarity of the different rare earth metals (see table 2). Furthermore, a variation of the surface sensitivity led to a similar assignment of the silicide nanowire components to their surface and deeper regions. Thereby, the R^* component was assigned to the wetting layer due to its exclusive observation at low Dy coverages.

To elucidate the possible influence of the wetting layer on the Si-2p nanowire spectra, we will discuss Si-2p spectra of the wetting layer in the following (see figure 7). For the complete coverage of the Si(001) surface with the wetting layer, Tb coverages of slightly less than 0.5 ML are necessary [10, 48]. Thus, we may assume that the wetting layer does not involve multiple layers, so that we expect the highest relative intensity of the Si-2p spectra of the wetting layer for the substrate component. This assignment of the substrate component leads to an estimation of the Fermi level position of about 0.65 eV above the valence band maximum and to Si-2p core-level shifts of the wetting layer as shown in table 2. Due to their very low relative intensities, we refrain from discussing the L^* and R_3 components.

Taking a closer look at the spectral components R^*, R_1, and R_2 of the wetting layer spectra, core level shifts very similar to the corresponding components of the nanowire Si-2p spectra are found. In contrast to the clear intensity differences of the nanowire spectral components (see above), the wetting layer spectral components have rather similar intensities (see figure 7(b)). This indicates that similar structural motives may be present in both structures, but also that the occurrence of such structural motives should be different. Regarding the influence of the wetting layer on the Si-2p nanowire spectra, it cannot be excluded that the R^* component of the nanowire spectra stems from the wetting layer in the vicinity of the nanowires. Nevertheless, the low intensity of the R^* component, the much higher intensities of the R_1 and R_2 components with respect to the R^* component, and the emergence of the additional R_3 and R_4 components with significant intensities in the case of the nanowire spectra clearly shows that the possible influence of the wetting layer on the nanowire Si-2p spectra is small.

Our Si-2p measurements demonstrate that the structure of the nanowires is independent of the vicinality of the substrate. Thus, the following findings from our ARPES measurements on vicinal samples will be also applicable to Tb silicide nanowires on planar Si(001) substrates.

3.3. Angle-resolved photoemission spectroscopy

An overview on the dispersion data of the electronic bands of a clean vicinal Si(001) substrate and of nanowires grown on the same substrate is shown in figure 8 for a large energy range. The ARPES data of the clean substrate are dominated by electronic bands of the Si bulk. In addition, a faint, but broad electronic band partially in the bulk band gap is observed and can be assigned to the Si dimers (red arrows in figures 8(a) and (b)) [49]. This band disperses slightly perpendicular to the step edges while no dispersion can be observed parallel to the step edges, which agrees with the orientation of the Si dimer rows on vicinal Si(001) substrates. In the following, $k_\perp$ stands for the in-plane surface momentum component perpendicular to the step edges and $k_\parallel$ represents the in-plane surface momentum component parallel to the step edges.

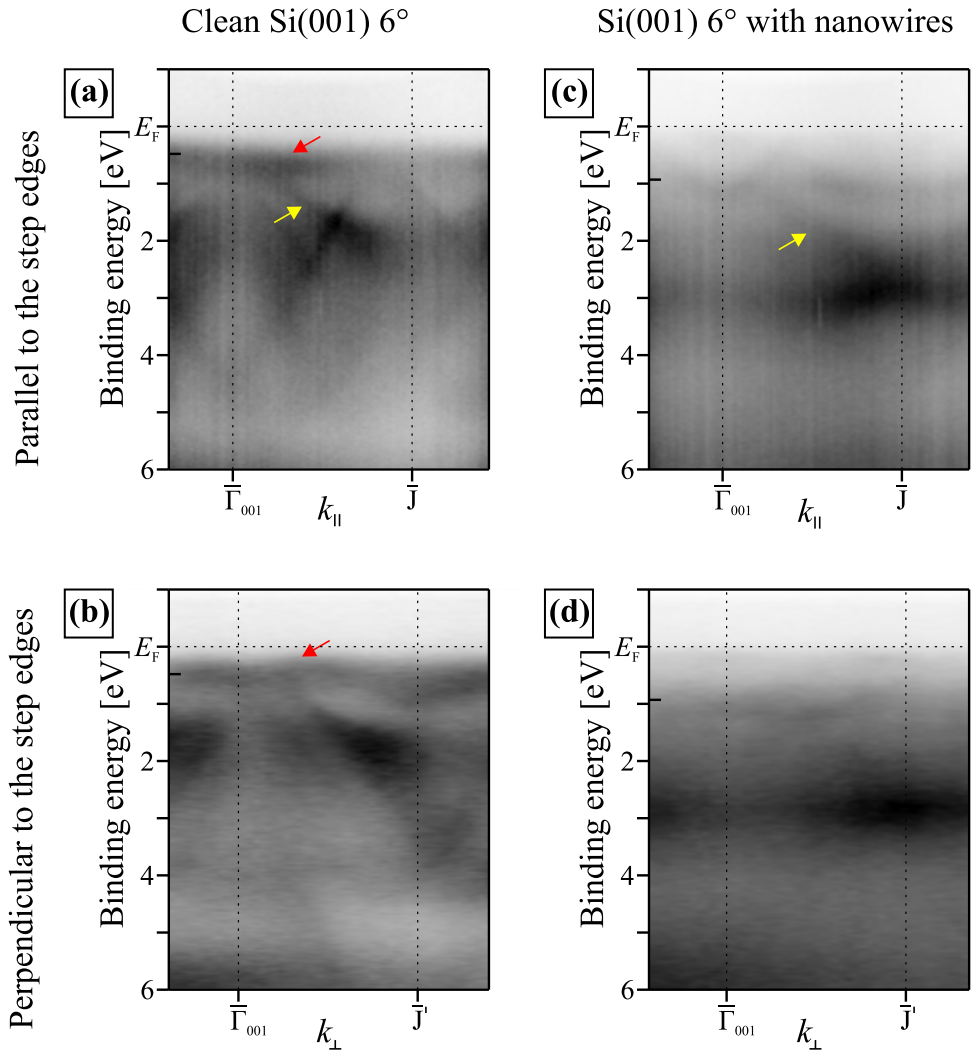

Figure 8. (a) and (b) dispersion plots of the electronic bands of the clean n-type Si(001) substrate with 6° offcut towards [110] and (c) and (d) of the same substrate with nanowires, (a) and (c) parallel and (b) and (d) perpendicular to the step edges ($h\nu = 62$ eV). The nanowires were prepared by deposition of 1.1 ML Tb and annealing at 600 °C (preparation 1). The Fermi level position was derived by determining the Fermi edge for the nanowire sample. $\overline{J}$ and $\overline{J}'$ are 8.2 nm^{-1} away from the Brillouin zone center ($\overline{\Gamma}_{001}$). The red arrows mark the band of the Si dimers of clean Si surfaces and the yellow ones indicate a Si bulk band that is observed prior and after the nanowire growth. The vertical stripes in (a) and (c) are artifacts of the spectrometer. The inside ticks on the binding energy scales indicate the substrate valence band maxima.

In contrast, this surface band as well as most Si bulk bands cannot be identified any more after the nanowire growth (see figures 8(c) and (d)). The surface band vanishes since most of the Si dimers disappear during the nanowire formation. The Si bulk bands lose intensity due to the additional structures on top of the surface and are broadened due to the non-homogeneous band bending, which also resulted in the increased Gaussian width for the *B* component of the nanowire samples in XPS (see section 3.2), so that almost no distinct bands are observable in the dispersion plots. Only the band marked by the yellow arrow in figure 8(a) can be clearly observed even for the sample with nanowires (see yellow arrow in figure 8(c)). The band is shifted down by about 0.4 eV for the nanowire sample, in good agreement with the change in band bending observed for the Si-2p substrate core-level.

The ARPES data of the nanowire sample are dominated by non-dispersing bands at about 2.8 eV and 5.8 eV binding energy (E_{Bin}), which presumably originate from the Tb-4f electrons and are observed in a similar manner also for Tb nanostructures on Si(111) [17]. Furthermore, there are electronic bands between the Fermi level and 1.0 eV binding energy, which therewith lie completely or at least partially in the substrate band gap. These bands can be unambiguously assigned to the Tb silicide nanowires since no dispersing bands could be found in this energy region for samples dominated by the wetting layer (not shown here) in agreement with findings for the Dy-induced wetting layer [25]. Close to the Fermi level, a very faint intensity is found around $\overline{\Gamma}_{001}$ and $\overline{J}$, although no distinct dispersion can be observed with the present contrast.

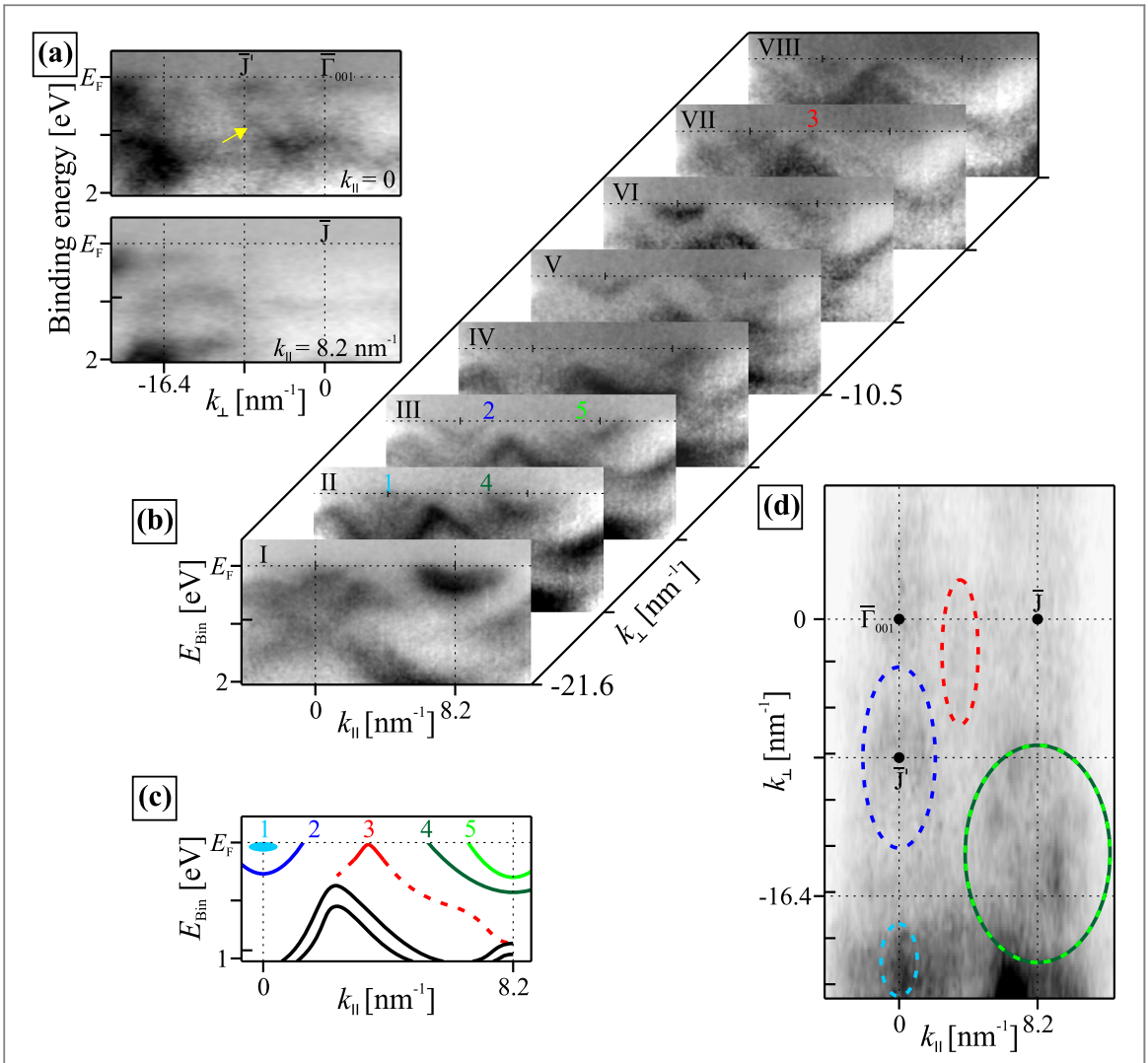

Figure 9. (a), (b), and (d) ARPES data of the nanowire sample also shown in figures 8(c) and (d) (preparation 1, $h\nu = 62$ eV). Detailed dispersion data around the Fermi level (a) perpendicular and (b) parallel to the step edges and (d) the Fermi surface. The yellow arrow in (a) marks a dispersing band. (c) Schematics of the average dispersion curves parallel to the nanowires of those bands touching or crossing the Fermi level, with the $k_\perp$-averaged binding energies and $k_{||}$ values as derived from the data. The dashed dispersion segments were not unambiguously detectable. In black, bands not reaching the Fermi level are indicated. The inside ticks in (a), (b), and (c) indicate the substrate valence band maximum, and the ones in (d) mark the positions where the dispersion plots shown in (b) were taken. The ellipses in (d) highlight areas of interest.

The region close to the Fermi level is shown in more detail in figures 9(a) and (b). For improving the contrast in these plots, the mean energy distribution curve, averaged over all measured $k_\perp$ and $k_{||}$, was subtracted from every single energy distribution curve for specific $k_\perp$ and $k_{||}$ values. Thereby, the mean energy distribution curve was weighted by the average intensity of the single energy distribution curve in order to reduce the vertical stripe pattern observed in figures 8(a) and (c). Furthermore, varying, nonlinear grayscales were used to highlight faint structures. It should be noted that the nanowire bands are rather broad and partially have a low visibility due to the unavoidable inhomogeneity of the samples, which are only partially covered by single and bundled nanowires of varying widths. Nevertheless, the present data allow us to track the nanowire bands in the full $k_\perp$–$k_{||}$-space.

Figure 9(a) shows the dispersion data perpendicular to the step edges and therewith to the nanowires through $\bar{\Gamma}_{001}$ ($k_{||} = 0$) and $\bar{J}$ ($k_{||} = 8.2$ nm^{-1}). There are dispersing electronic bands even in the substrate band gap, e.g. the band marked with a yellow arrow in figure 9(a), meaning that these bands can be assigned to the nanowires. This behavior already indicates that the nanowires are not a completely one-dimensional electronic system with purely one-dimensional dispersion, as it is also expected for real world systems. Such a behavior can be characteristic for single nanowires, but could also arise due to coupling with neighboring nanowires in bundles or with the surrounding. Still, their electronic structure may be quasi one-dimensional when only oscillating lines are observed in the energy contours of the nanowire bands, instead of closed curves, such as circles or ellipses, as will be investigated in detail further below. In addition to dispersing bands in the substrate

Table 3. Overview on the $k_\perp$-averaged binding energies of the bottoms of the bands and effective masses for the parabolic bands around $k_\parallel = 0$ and $k_\parallel = 8.2$ nm^{-1} (bands 2, 4, and 5) and the values reported in the literature [24, 25]. Preparation 1–3 are the ones of which ARPES data are shown in figures 9, 10(a), and 11, respectively. The effective masses (m^*) are given in units of m_0 and the $k_\perp$-averaged binding energies of the bottoms of the bands (E^{Bot}) in eV.

	E_2^{Bot}	$m^*{}_2$	E_4^{Bot}	$m^*{}_4$	E_5^{Bot}	$m^*{}_5$
Preparation 1 (figure 9)	0.25 ± 0.05	0.25 ± 0.05	0.45 ± 0.05	0.7 ± 0.1	0.30 ± 0.05	0.4 ± 0.1
Preparation 2 (figure 10(a))	0.31 ± 0.05	0.24 ± 0.05	0.4 ± 0.1	1.0 ± 0.5	0.3 ± 0.1	0.2 ± 0.1
Preparation 3 (figure 11)	0.24 ± 0.05	0.19 ± 0.05	0.43 ± 0.05	0.6 ± 0.1	—	—
$DySi_2$ and $ErSi_2$ nanowires [25]	0.38 ± 0.05	0.2 ± 0.1	0.53 ± 0.05	1.1 ± 0.2	0.26 ± 0.05	1.0 ± 0.3
$GdSi_2$ nanowires [24]	—	—	—	0.91 ± 0.05	—	0.63 ± 0.05

band gap, strong intensity variations, but without clear dispersion are observed directly at the Fermi level in figure 9(a).

Parallel to the step edges, dispersing bands reaching the Fermi level are clearly observed (see figure 9(b)). Intensity variations are also apparent in the dispersion plots for various values of $k_\perp$, e.g. for the feature at $k_\parallel = 0$ starting with a slowly diminishing intensity (panels I–III), followed by no significant intensity observed any more (panel IV), an intensity increase (panels V and VI), and again a decrease (panels VII and VIII). These intensity variations may be due to strong matrix element effects.

Taking a closer look at figure 9(b), five electronic bands with intensity at the Fermi level can be distinguished (labeled 1–5 in figure 9(b) and schematically drawn in figure 9(c)). Band 1 lies exactly at $k_\parallel = 0$ in close vicinity to the Fermi level (light blue in figure 9(c)), enclosed by the parabolic band 2. A similar band 1 was also observed by Yeom *et al* for Gd silicide nanowires and they did not observe a clear crossing of the Fermi level of this band [24]. Here, the Fermi surface of the nanowire sample shows a high intensity at $k_\parallel = 0$ for high negative values of $k_\perp$, so that we assume that this band crosses or at least reaches the Fermi level (see light blue ellipse in figure 9(d)). It may also be present in the data of Wanke *et al* since they reported rather filled appearing parabolas for band 2 even though they did not mention it specifically [25]. However, the characteristics of band 1 as electron-like or hole-like remains unclear up to now since no dispersion is observed. An electron-like characteristics is possible, where the bottom of the band lies closely below the Fermi level. On the other hand, a possible hole-like characteristics would be superposed by band 2.

Band 2 clearly shows an electron-like behavior (dark blue in figure 9(c)). Analyzing its contour at the Fermi surface, it appears to be quasi one-dimensional since two almost straight lines symmetric to $k_\parallel = 0$ are observed that do not form a closed curve even though they may oscillate slightly, e.g. in the area marked by the dark blue circle in figure 9(d). Due to the oscillation, the determination of its maximum binding energy, i.e. the binding energy of the bottom of the band, and its curvature is rather uncertain, but the $k_\perp$-averaged binding energy of the bottom of band 2 is $E_2^{\mathrm{Bot}} = (0.25 \pm 0.05)$ eV and its average effective mass is $m_2^* = (0.25 \pm 0.05)\ m_0$, where m_0 is the free electron mass (see table 3). It should be noted that no corresponding band 2 crossing the Fermi level was reported for Gd silicide nanowires [24], even though a similar electronic structure is expected for all rare earth silicide nanowire systems due to the electronic similarities of the trivalent rare earth metals. However, assuming a similar intensity variation of the electronic bands for the Gd silicide nanowires as observed here, the non-observation of this band may be simply due to measurements at a $k_\perp$ where its intensity is too low since no data of a variation of $k_\perp$ were reported around $k_\parallel = 0$ [24].

Band 3 with intensity at or close to the Fermi level was never observed before, again possibly due to the missing systematic variation of $k_\perp$ in prior studies (red in figure 9(c)). It reaches the Fermi level forming a rather sharp kink (see figure 9(b) panel VII). Thus, it has hole-like characteristics, but we do not estimate its effective mass since the assumption of a parabola for such a linear dispersion is inappropriate. From its appearance on the Fermi surface (see red ellipse in figure 9(d)), we may conclude that it is quasi one-dimensional since only a linear feature is observed. Interestingly, a band crossing the Fermi level at approximately the same $k_\parallel$-position as band 3 was expected from a comparison of the silicide nanowire band structure on Si(001) with the band structure of the two-dimensional silicide film on Si(111) [50].

The further two electronic bands 4 and 5 crossing the Fermi level are centered around the edge of the first Brillouin zone ($k_\parallel = 8.2$ nm^{-1}) and were also found in prior ARPES studies for Gd, Dy, and Er silicide nanowires (dark and light green curves in figure 9(c), respectively) [24, 25]. While they appear as one broad feature in figure 9(b) panel I, as also reported in an early study for Dy silicide nanowires [51], two distinguished bands are seen in the further dispersion plots (see figure 9(b) panels II–VII) and at the Fermi surface, e.g. in the area marked by a green ellipse in figure 9(d). Their contour at the Fermi surface also reveals the quasi one-dimensional nature of these electronic bands since only oscillating lines, but no closed curves are observed. Analyzing the band dispersions in detail, we find $E_4^{\mathrm{Bot}} = (0.45 \pm 0.05)$ eV, $m_4^* = (0.7 \pm 0.1)\ m_0$, $E_5^{\mathrm{Bot}} = (0.30 \pm 0.05)$ eV, and $m_5^* = (0.4 \pm 0.1)\ m_0$. Similar as for band 2, only average values can be given

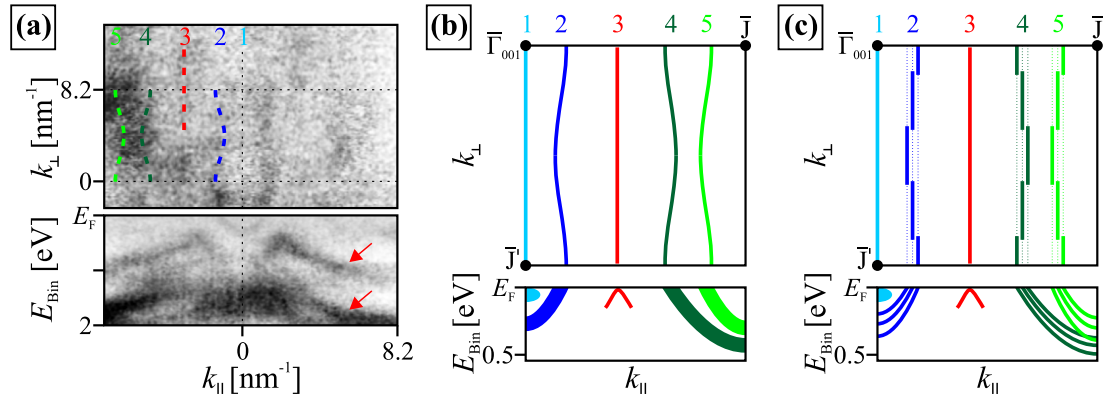

Figure 10. (a) Fermi surface (top) and detailed dispersion around the Fermi level parallel to the nanowires at $k_\perp = -2.4$ nm^{-1} (bottom) for another nanowire sample (preparation 2: Si(001) substrate with 6° offcut towards [110]; 1.2 ML Tb and annealing at 550 °C; $h\nu = 62$ eV). The zero of $k_\perp$ is set to agree with the data of preparation 1 since no Si bulk bands were clearly distinguishable for calibration in the present case. The colored dashed lines are guides to the eyes. The red arrows indicate nearly parallel bands. (b) Schematics of the possible oscillating contours at the Fermi surface (top) and corresponding dispersion curves (bottom) of the five bands crossing or reaching the Fermi level not taking into account their intensity variations. The uncertainties due to the variation of the dispersion with $k_\perp$ is illustrated by thick curves. In (c), the possible effects of a combination of different purely one-dimensional bands with strong matrix element effects is shown. For the illustration of the inhomogeneity of the dispersion curves, the effective masses of the bands are set constant and only the binding energies of the bottoms of the bands vary.

since the contours at the Fermi surface of bands 4 and 5 are slightly oscillating with varying $k_\perp$ (see green ellipse in figure 9(d)). Such an oscillation of band 4 was also reported for Gd silicide nanowires [24].

A more pronounced oscillation in a contour at the Fermi surface is observed for band 2 centered around $k_{||} = 0$ at a different nanowire sample (see figure 10(a)), although the preparation conditions were rather similar to the ones of the sample discussed above. Here, a clear increase, decrease and again increase of the distance between the curves of this band is observed with increasing $k_\perp$ before its signal vanishes. Interestingly for this sample, the electronic band 1 is not observed for any $k_\perp$, while all other previously discussed bands are found. Moreover, the bands 3–5 appear rather broad, in contrast to the sharpness of band 2, leading to rather high uncertainties regarding the binding energies of the bottoms of the bands and the effective masses for the bands 4 and 5. This broadness could be related to an inhomogeneity of the nanowire widths or the bundle size for this specific sample. The determined $k_\perp$-averaged parameters for the electronic bands 2, 4, and 5 are listed in table 3.

Another interesting aspect of the dispersion shown in the lower part of figure 10(a) is the observation of nearly parallel bands at higher binding energies, which are separated by about 1 eV (marked by red arrows). These electronic bands do not only show a similar dispersion in $k_{||}$ direction for this particular $k_\perp$, but also disperse similarly in $k_\perp$ direction, as it is nicely seen in the ARPES data of another nanowire sample shown in figure 11. Despite their dispersion parallel and perpendicular to the step edges (see figures 11(a) and (b)), these electronic bands have contours at the constant-energy surface characterized by only slightly oscillating lines symmetric to $k_{||} = 0$ demonstrating their quasi one-dimensional characteristics (see bottom of figure 11(c)). This indicates that not only the bands close to the Fermi level show a quasi one-dimensional behavior, but also deeper lying nanowire bands.

For the ARPES data shown in figure 11, nanowires were grown on a Si(001) substrate with an offcut of 4° towards [110] in contrast to the previously discussed nanowire samples (6° offcut towards [110]). In general, the same electronic structure is observed, again confirming that identical nanowires grow on the various Si(001) substrates (see figures 9, 10(a), and 11). The parabolic band 2 is found around $k_{||} = 0$ (see figure 11(b) panels I–III, V, and VI), which appears filled for certain values of $k_\perp$ indicating the existence of the electronic band 1 (see figure 11(b) panels V and VI and (c)). The electronic bands 3 and 5 appear faintly in figure 11(b) panel II (red and light green dashed circles, respectively), but they cannot be recognized at the Fermi surface for this preparation. In contrast, band 4 is nicely observed in both the dispersion plots and at the Fermi surface. The $k_\perp$-averaged binding energies of the bottoms of the bands and $k_\perp$-averaged effective masses of the bands 2 and 4 are listed in table 3.

Comparing the determined binding energies of the bottoms of the bands and effective masses of the same electronic bands, there is a nice agreement of all preparations (see table 3). Slight differences, as observed for the binding energies of the bottom of band 2, are expected since different ensembles of a variety of nanowires (single and bundled nanowires of varying widths, which all may have a slightly different electronic structure) are probed resulting in different average electronic structures observed. The probing of nanowire ensembles may also

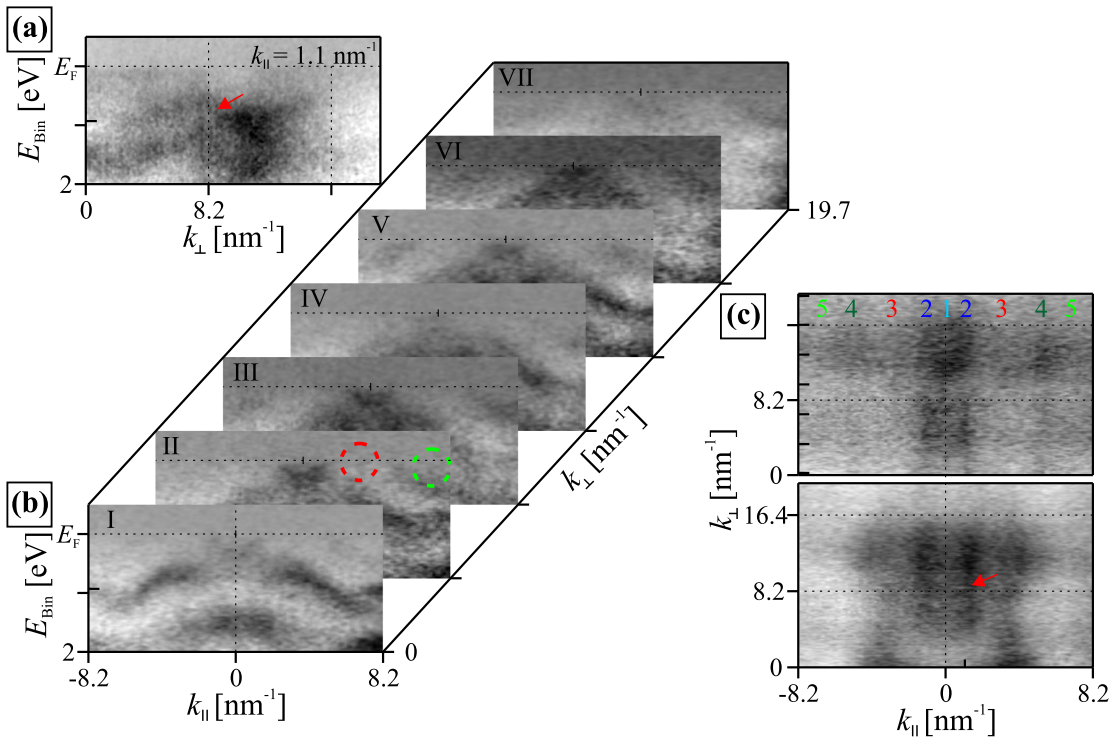

Figure 11. ARPES data of the nanowire sample on n-type Si(001) with 4° offcut towards [110], for which the Si-2p spectrum was shown in figure 6(a) (preparation 3: 1.5 ML Tb and annealing at 550 °C; $h\nu = 62$ eV). The zero of $k_\perp$ is arbitrary since neither substrate bands nor clear oscillations of the contours at the Fermi surface were observed. (a) and (b) detailed dispersion data near the Fermi level (a) perpendicular and (b) parallel to the step edges. The inside ticks on the binding energy scales indicate the substrate valence band maximum. (c) Energy surface at the Fermi level (top) and at $E_{Bin} = 0.7$ eV (bottom). The red arrows in (a) and (c) mark the same electronic band, and the inside ticks in (c) mark the positions where the dispersion plots in (a) and (b) were taken.

explain why some bands are absent for certain preparations since the specific nanowire structures contributing strongly to these bands may be missing.

The significant differences of our determined binding energies of the bottoms of the bands and effective masses compared with the available literature values for nanowires from other rare earth elements (see table 3) cannot be explained by the probing of nanowire ensembles alone, even though slight growth differences are known, e.g. increased bundle formation for certain rare earth elements [14, 24, 25]. Especially, the large variations of the effective masses of the electronic bands centered around $k_{||} = 8.2$ nm^{-1} (bands 4 and 5) indicate a more direct influence of the used rare earth metal on the detailed electronic structure. Nevertheless, some general trends can be observed. The effective mass of band 2 is smaller than the ones derived for the bands 4 and 5. Furthermore, a higher effective mass for the band 4 than for band 5 was observed in all measurements up to now. Finally, the general electronic structures are very similar for all rare earth silicide nanowires on Si(001). The electronic bands 1, 4, and 5 observed for Tb disilicide nanowires were also found for Gd silicide nanowires, and the electronic bands 2, 4 and 5 were also found for Dy and Er silicide nanowires [24, 25]. Thereby, the non-observation of all bands observed here in the studies of the other rare earth elements may be due to the missing systematic variation of $k_\perp$. Thus, we may assume that the quasi one-dimensional signatures of nearly linear and only slightly oscillating energy contours, especially at the Fermi level, are universal for all trivalent rare earth silicide nanowires on Si(001) consisting of hexagonal rare earth disilicides.

Figure 10(b) summarizes schematically our findings regarding the electronic dispersion and the Fermi surface of Tb silicide nanowires. The schematic Fermi surface depicts the oscillations of the contours at the Fermi surface of the bands 2, 4, and 5 as observed in particular for preparation 2 (see figure 10(a)). Thereby, the contours at the Fermi surface of band 2 has its maximum $k_{||}$ at $k_\perp = 0$ in agreement with the observation for preparation 1 (see figure 9(d)).

While the oscillations of the contours at the Fermi surface are not clearly resolved for all bands, the contour at the Fermi surface of band 2 clearly appears as an oscillating line for preparation 2 indicating a coupling within a nanowire, between neighboring nanowires in a bundle, or of nanowires with their surrounding (see figure 10(a)). Nevertheless, we cannot exclude that the oscillating appearance stems from the measurement of inhomogeneous nanowire ensembles. The nanowires may have purely one-dimensional, but slightly different electronic structures depending on their width as well as on their formation as single or bundled nanowires,

resulting in different straight lines as contours at the Fermi surface. Now an oscillating appearance may result from matrix element effects leading to dominant intensities of different nanowires at certain values of $k_\perp$. Such a scenario is exemplarily shown in figure 10(c). Strong matrix element effects are already evident due to the strong intensity variations of the bands with $k_\perp$. However, both scenarios and also a combination of them are possible based on the present data.

Finally it should be noted that the present experimental results alone do not allow to assign the five observed bands to specific atoms or building blocks of the nanowires. On the other hand, theoretical studies could shed light on this issue and could also explain the varying visibility of certain bands in the ARPES experiments. Moreover, the consequences of spin-orbit effects on the bands, which are frequent in rare earth systems, could be clarified. Therefore detailed theoretical studies on these fascinating nanowire systems are highly desirable.

4. Summary and conclusion

We studied the electronic structure of Tb silicide nanowires by STS, XPS, and ARPES. Thereby, a metallic behavior was observed for all nanowires using STS. Si-2p spectra showed the same main components for nanowires on planar and vicinal substrates with various offcut angles indicating the growth of identical nanowires independent of the substrate vicinality. Furthermore, a Fermi level position near the conduction band minimum (about 0.93 eV above the valence band maximum) was found supporting the present structure model based on hexagonal Tb disilicide. Moreover, such an extreme Fermi level position resulting in a high Schottky barrier height on p-type Si is a prerequisite for applications as electrically isolated nanowires in Si-based nanoelectronics.

Five electronic bands crossing or reaching the Fermi surface were observed in our ARPES experiments. Their contours at the Fermi surface showed quasi one-dimensional characteristics consisting of straight or only slightly oscillating lines in the direction perpendicular to the nanowires. This verifies the assumption that Tb silicide nanowires on Si(001) are quasi one-dimensional metals. In addition to the oscillation of the contours at the Fermi surface also strong variations of the band intensities were found indicating strong matrix element effects. Due to these uncertainties, an exact determination of the bands dispersion was not possible, but some general parameters could be determined, e.g. the average binding energies at the bottoms of the bands and the average effective masses. The values obtained in this way reproduce trends also observed for other rare earth silicide nanowire systems on Si(001) [24, 25]. Also, the general electronic structure found for other rare earth silicide nanowires is nicely reproduced and the observed differences are assigned to the intensity variations of the bands due to strong matrix element effects leading to their non-observation at certain $k_\perp$ values. Thus, the observation of a quasi one-dimensional metallicity should not be an exclusive feature for the Tb silicide nanowires investigated here, but rather should represent a general feature of rare earth silicide nanowires on Si(001).

Acknowledgments

We thank K Horn for providing the chamber system for the photoemission experiments and BESSY II (Helmholtz-Zentrum Berlin) for providing the beamtimes. R Koch, S Böttcher, H Vita, J Döhring, C Prohl, Z Diemer, and L Freter are acknowledged for their support during the measurements. This work was funded by the Deutsche Forschungsgemeinschaft through FOR 1700 project E2.

References

[1] Tomonaga S 1950 *Prog. Theoret. Phys.* **5** 544
[2] Luttinger J M 1963 *J. Math. Phys.* **4** 1154
[3] Peierls R E 1955 *Quantum Theory of Solids* (Oxford: Oxford University Press)
[4] Kagoshima S 1981 *Japan J. Appl. Phys.* **20** 1617
[5] Zeng C, Kent P R C, Kim T H, Li A P and Weitering H H 2008 *Nat. Mater.* **7** 539
[6] Snijders P C and Weitering H H 2010 *Rev. Mod. Phys.* **82** 307
[7] Blumenstein C, Schäfer J, Mietke S, Meyer S, Dollinger A, Lochner M, Cui X, Patthey L, Matzdorf R and Claessen R 2011 *Nat. Phys.* **7** 776
[8] Aulbach J, Schäfer J, Erwin S C, Meyer S, Loho C, Settelein J and Claessen R 2013 *Phys. Rev. Lett.* **111** 137203
[9] Edler F, Miccoli I, Demuth S, Pfnür H, Wippermann S, Lücke A, Schmidt W G and Tegenkamp C 2015 *Phys. Rev.* B **92** 085426
[10] Appelfeller S, Kuls S and Dähne M 2015 *Surf. Sci.* **641** 180
[11] Preinesberger C, Vandré S, Kalka T and Dähne-Prietsch M 1998 *J. Phys. D: Appl. Phys.* **31** L43
[12] Chen Y, Ohlberg D A A, Medeiros-Ribeiro G, Chang Y A and Williams R S 2000 *Appl. Phys. Lett.* **76** 4004
[13] Nogami J, Liu B Z, Katkov M V, Ohbuchi C and Birge N O 2001 *Phys. Rev.* B **63** 233305
[14] Chen Y, Ohlberg D A A and Williams R S 2002 *J. Appl. Phys.* **91** 3213
[15] Cui Y and Nogami J 2011 *Surf. Sci.* **605** 2038

[16] Vandré S, Kalka T, Preinesberger C and Dähne-Prietsch M 1999 *Phys. Rev. Lett.* **82** 1927
[17] Franz M, Appelfeller S, Prohl C, Große J, Jirschik H-F, Füllert V, Hassenstein C, Diemer Z and Dähne M 2016 *J. Vac. Sci. Technol.* A **34** 061503
[18] Sanna S, Dues C, Schmidt W G, Timmer F, Wollschläger J, Franz M, Appelfeller S and Dähne M 2016 *Phys. Rev.* B **93** 195407
[19] Vandré S, Preinesberger C, Busse W and Dähne M 2001 *Appl. Phys. Lett.* **78** 2012
[20] Appelfeller S, Franz M, Kubicki M, Reiß P, Niermann T, Schubert M A, Lehmann M and Dähne M 2016 *Appl. Phys. Lett.* **108** 013109
[21] Ohbuchi C and Nogami J 2002 *Phys. Rev.* B **66** 165323
[22] Qin S, Kim T H, Zhang Y, Ouyang W, Weitering H H, Shih C K, Baddorf A P, Wu R and Li A P 2012 *Nano Lett.* **12** 938
[23] Miccoli I, Edler F, Pfnür H, Appelfeller S, Dähne M, Holtgrewe K, Sanna S, Schmidt W G and Tegenkamp C 2016 *Phys. Rev.* B **93** 125412
[24] Yeom H W, Kim Y K, Lee E Y, Ryang K D and Kang P G 2005 *Phys. Rev. Lett.* **95** 205504
[25] Wanke M, Löser K, Pruskil G, Vyalikh D V, Molodtsov S L, Danzenbächer S, Laubschat C and Dähne M 2011 *Phys. Rev.* B **83** 205417
[26] Horcas I, Fernández R, Gómez-Rodríguez J M, Colchero J, Gómez-Herrero J and Baro A M 2007 *Rev. Sci. Instrum.* **78** 013705
[27] Preinesberger C, Becker S K, Vandré S, Kalka T and Dähne M 2002 *J. Appl. Phys.* **91** 1695
[28] Lang N D 1986 *Phys. Rev.* B **34** 5947
[29] Stroscio J A, Feenstra R M and Fein A P 1986 *Phys. Rev. Lett.* **57** 2579
[30] Iancu V, Kent P R C, Hus S, Hu H, Zeng C G and Weitering H H 2013 *J. Phys.: Condens. Matter* **25** 014011
[31] Landemark E, Karlsson C J, Chao Y C and Uhrberg R I G 1992 *Phys. Rev. Lett.* **69** 1588
[32] Koh H, Kim J W, Choi W H and Yeom H W 2003 *Phys. Rev.* B **67** 073306
[33] Eriksson P E J and Uhrberg R I G 2010 *Phys. Rev.* B **81** 125443
[34] Vandré S 2000 *Growth and Electronic Structure of Lanthanide Silicides on Si(111) and Si(001)* (Berlin: Wissenschaft und Technik Verlag)
[35] Shinotsuka H, Tanuma S, Powell C J and Penn D R 2015 *Surf. Interface Anal.* **47** 871
[36] Hamers R J 1988 *J. Vac. Sci. Technol.* B **6** 1462
[37] Schofield S R, Studer P, Hirjibehedin C F, Curson N J, Aeppli G and Bowler D R 2013 *Nat. Commun.* **4** 1649
[38] Little E J Jr. and Jones M M 1960 *J. Chem. Educ.* **37** 231
[39] Vandré S, Kalka T, Preinesberger C and Dähne-Prietsch M 1999 *J. Vac. Sci. Technol.* B **17** 1682
[40] Chandola S, Speiser E, Esser N, Appelfeller S, Franz M and Dähne M 2016 unpublished
[41] Himpsel F J, Meyerson B S, McFeely F R, Morar J F, Taleb-Ibrahimi A and Yarmoff J A 1990 Core level spectroscopy at silicon surfaces and interfaces *Proc. Int. School of Physics 'Enrico Fermi' CVIII—Photoemission and Absorption Spectroscopy of Solids and Interfaces with Synchrotron Radiation*ed M Campagna and R Rosei (Amsterdam: Elsevier) p 203
[42] Kentsch C, Kutschera M, Weinelt M, Fauster T and Rohlfing M 2001 *Phys. Rev.* B **65** 035323
[43] Tersoff J 1984 *Phys. Rev. Lett.* **52** 465
[44] Flores F and Tejedor C 1987 *J. Phys. C: Solid State Phys.* **20** 145
[45] Bechstedt F and Scheffler M 1993 *Surf. Sci. Rep.* **18** 145
[46] Schottky W 1938 *Naturwissenschaften* **26** 843
[47] Bulanova M, Mikolenko A, Meleshevich K, Effenberg G and Saltykov P 1999 *Z. Metallkd.* **90** 216
[48] Liu B Z and Nogami J 2003 *Surf. Sci.* **540** 136
[49] Johansson L S O, Uhrberg R I G, Mårtensson P and Hansson G V 1990 *Phys. Rev.* B **42** 1305
[50] Dähne M and Wanke M 2013 *J. Phys.: Condens. Matter* **25** 014012
[51] Preinesberger C, Pruskil G, Becker S K, Dähne M, Vyalikh D V, Molodtsov S L, Laubschat C and Schiller F 2005 *Appl. Phys. Lett.* **87** 083107